Design and Test of an Optical Transition Radiation Beam Monitor for the T2K Experiment

By Brian Kirby

Abstract

An Optical Transition Radiation (OTR) beam monitor design is presented as a means to detect the width and position of the T2K proton beam. The temperature rise and steady state temperature of the foil component is studied and it is concluded that Titanium alloy or graphite foils would be suitable. Optical simulations suggest that the design can image particle beams and has a suitably uniform light acceptance (less then 10 % variation) over the surface of the foil component and small blurriness. The test of a prototype of the system is described, and the system is found to be able to detect OTR light and image particle beams. It is recommended that the OTR beam monitor be considered for use as the proton beam monitor in the target station of the T2K experiment.

Acknowledgments

I would like to thank Carl Ross and the National Research Council for their invaluable help and the use of their facilities.

T2K OTR Detector - Introduction

An Optical Transition Radiation (OTR) beam monitor uses light emitted when a proton beam passes through a thin foil to observe and measure the particle beam's position and profile accurately. This type of detector has been used extensively with electron beams and has been studied for use in the Tevatron at Fermilab [1]. This report will determine the feasibility of using an OTR detector to monitor the T2K proton beam in the target station. The principle advantages of the OTR monitor for this application is that it is simple and resistant to radiation damage.

Neutrino Oscillations and The T2K Experiment

Neutrino Oscillations in the Standard Model

The neutrino is a Dirac fermion with no electric or colour charge that participates only in the weak interaction. Each lepton family has a neutrino and anti-neutrino(ν_e,ν_μ and ν_τ) that interacts with the associated charged lepton. The recent observation of oscillations between neutrino flavours suggests that the neutrinos have mass and that the weak interaction states are a superposition of the mass states. This is similar to the Cabibbo theory of flavour-mixing of quark states in the weak interaction. The mixing of neutrino states is parameterized by the Maki-Nakagawa-Sakata matrix as [MNS]

$$\begin{pmatrix} \nu_e \\ \nu_\mu \\ \nu_\tau \end{pmatrix} = U \begin{pmatrix} \nu_1 \\ \nu_2 \\ \nu_3 \end{pmatrix}$$

with

$$U = \begin{pmatrix} 1 & 0 & 0 \\ 0 & \cos\theta_{23} & \sin\theta_{23} \\ 0 & -\sin\theta_{23} & \cos\theta_{23} \end{pmatrix} \begin{pmatrix} \cos\theta_{13} & 0 & \sin\theta_{13}e^{-i\delta} \\ 0 & 1 & 0 \\ -\sin\theta_{13}e^{i\delta} & 0 & \cos\theta_{13} \end{pmatrix} \begin{pmatrix} \cos\theta_{12} & \sin\theta_{12} & 0 \\ -\sin\theta_{12} & \cos\theta_{12} & 0 \\ 0 & 0 & 1 \end{pmatrix}$$

This mixing-matrix is unitary and CP-violating phase is apparent. The principle goal of neutrino oscillation experiments is to measure the neutrino oscillation parameters which are experimental constants in the standard model.

The T2K Experiment

The T2K experiment is the successor to the K2K experiment and is designed to measure θ_{23} and Δm^2_{23} to unprecedented accuracy. The discovery of θ_{13} or the measurement of its upper limit are also physics goals.

The neutrino mixing angles are measured by producing a neutrino beam and measuring the neutrino flavour flux at two different points along its path. The oscillation parameters can be deduced from the change in neutrino flux and the distance between measurement points. In the case of T2K the two detectors are the Super-Kamiokande detector and a detector to be built at J-PARC (the far and near detectors respectively). The probability of ν_μ to ν_e oscillation (assuming oscillation to ν_{tau} is negligible) is given approximately by [2]:

$$P(\nu_\mu \rightarrow \nu_e) = \sin^2 2\theta_{13} \sin^2\theta_{23} \sin^2\Phi_{23}$$
$$\Phi_{23} = \Delta m^2_{23} L/4E_\nu$$

with L the distance between the two detectors and E_ν the neutrino energy. For T2K L is 295 km and a neutrino energy of roughly 0.8 GeV is chosen in order to maximize the oscillation probability, assuming a Δm^2_{23} or roughly 0.003 eV^2

The neutrino beam is produced at the J-PARC facility by colliding protons into a graphite target in order to produce pions, obtaining a neutrino beam when the pions decay into neutrinos. T2K uses an off-axis beam which allows the energy spectrum of the particles incident on the detectors to be modified by varying the angle of the measured neutrino flux with the initial proton beam direction. By selecting an off-axis angle the measured energy spectrum is narrowed while maximizing the number of neutrinos at the desired energy. [1]

The off-axis neutrino beam design requires the initial proton/pion beam direction to be precisely measured to ensure the correct off-axis angle is incident on the detectors. For this reason it would be useful to have a proton beam monitor directly in front of the pion production target which in conjunction with upstream monitors would measure the proton beam position and direction. A position resolution of less then 1mm is required to ensure the energy spectrum is within acceptable limits. A beam monitor is also needed to protect the target from an over focused beam.

Figure 1: T2K Target Station

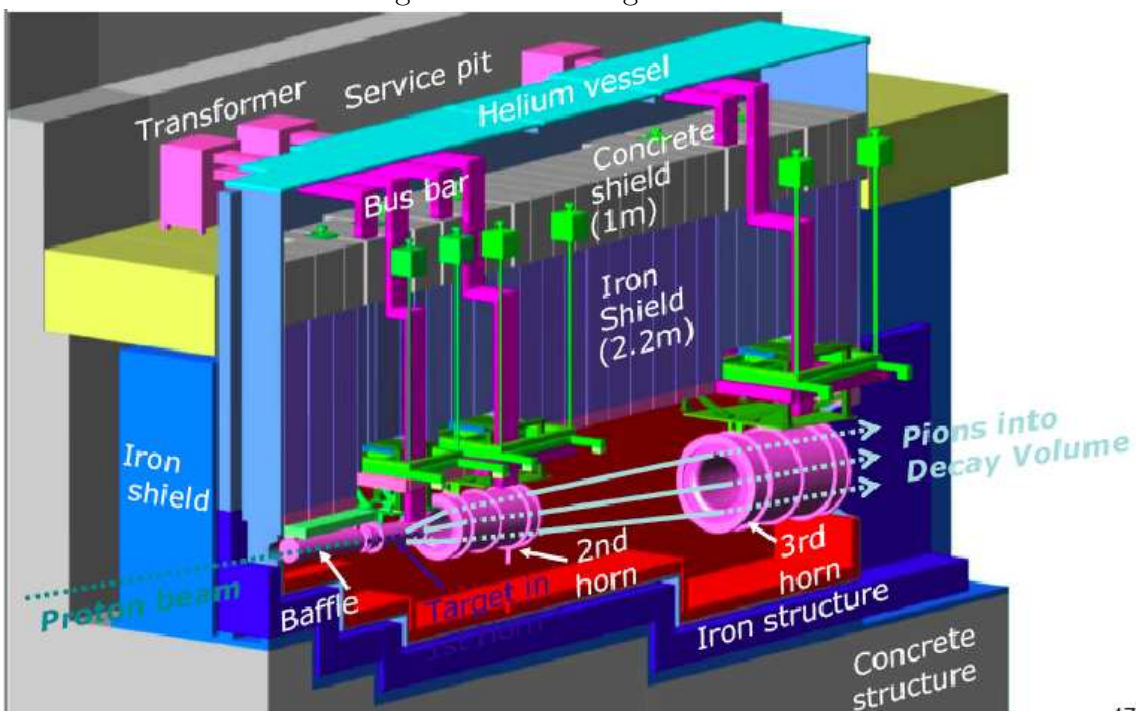

Optical System Design - System Requirements

The OTR detector is required to image the proton beam with a position resolution of better than 1mm and to measure the beam width to within 7 %. It must be resistant to radiation damage and so cannot include glass components or place electronics in high radiation areas. Finally the system must last longer than two years without maintenance due to the expense of retrieving it from the target station replacing it.

The design of the optical system is also constrained by the physical layout of the target station, shown in Figure 1. The OTR detector will be placed between the collimating baffle and target and transition radiation must be carried through the shielding above the production target and through the helium lid before a camera can be used. The channel that the light passes through must be as small as possible to prevent excessive radiation leakage out of the shielding. The system cannot use glass optics to focus the light when it passes through the light pipe which requires focalizing mirrors to be used instead.

System Design

The optical system consists of four parabolic mirrors that transport the transition radiation emitted off a foil positioned in the path of the proton beam. The radiation is transported through the target station shielding up to the camera unit placed on top of the helium lid.

Figure 2: OTR Optical System Design

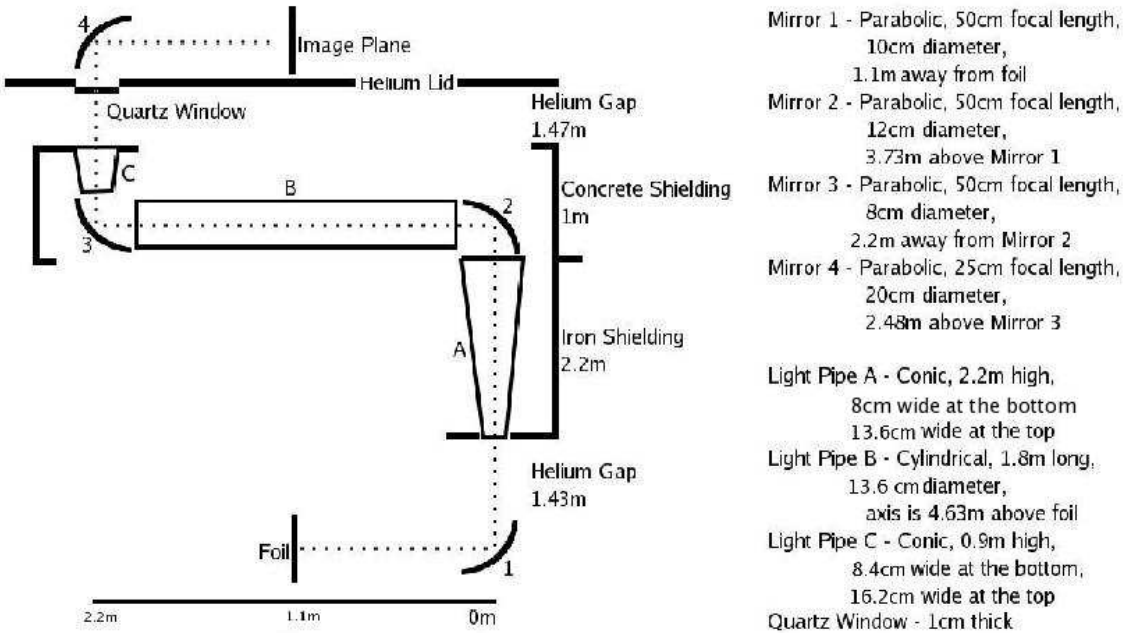

The precise mirror positions are depicted in Figure 2. The OTR foil ladder contains multiple foils so that damaged foils can be replaced without removing the target station shielding. A quartz window allows light to pass through the helium lid.

Foil Temperature and Thermal Stress - Introduction

The T2K beam will be very intense (approximately 3.3×10^{14} protons per pulse, 3.2 sec between pulses [2]), raising the possibility that the OTR foil may be destroyed by thermal stress or melting. The OTR detector design is feasible only if estimates show the temperature rise in the foil and its steady state temperature are sufficiently low.

Temperature Rise and Thermal Stress in the OTR Detector Foil - Hand Calculation

The T2K particle beam is pulsed with each pulse shape approximately Gaussian in the directions transverse to its velocity. By assuming a co-ordinate system with an origin at the centre of the beam and the x and y axis pointed in the transverse directions, the differential intensity dI of the particle beam in an infinitesimal region can be written as:

$$dI = Ne^{-(x^2+y^2)/2\sigma^2} dxdy$$

this being the number of particles that passes through the differential area $dxdy$ when a single pulse passes. The total intensity is found by integrating over the x-y plane:

$$I = \int\int_A Ne^{-(x^2+y^2)/2\sigma^2} dxdy$$

and as the intensity is known the normalization constant N is found to be

$$N = \frac{I}{2\pi\sigma^2}$$

The particle beam is incident on the OTR detector foil. When considering thermal effects on the foil, it is useful to define a foil co-ordinate system with its origin at the point that the centre of the particle beam hits the foil, and the x' and y' axis constrained to lie on the foil's surface. The foil may by some angle θ to the transverse plane of the beam; for simplicity the angle will be due to a rotation of the foil only about the y' axis. In this case, the relation between co-ordinates in either system are: $y' = y, x' = x/cos\theta$

In the foil co-ordinate system:

$$I = \int\int_{A'} N'e^{-(x'^2cos^2\theta+y'^2)/2\sigma^2} dx'dy'cos\theta$$

and:

$$dI' = N'e^{-(x'^2cos^2\theta+y'^2)/2\sigma^2} dx'dy'cos\theta \text{ with } N' = \frac{I}{2\pi\sigma^2}$$

When the proton beam passes through the foil it deposits energy through inelastic collisions[3]. The energy deposited in any differential area is:

$$dE_{dep} = dI'(\frac{dE}{dx})(\frac{t}{cos\theta})$$

with the dE/dx term being the Bethe-Bloche formula for the differential energy lost by a particle as it passes through matter:

$$\frac{dE}{dx} = -2\pi N_a r_e^2 m_e c^2 \rho \frac{Z}{A} \frac{z^2}{\beta^2} [ln(\frac{2m_e\gamma^2c^2\beta^2W_{max}}{I^2}) - 2\beta^2 - \delta] \text{ [3]}$$

A key assumption is that the energy lost by a proton as it passes through the foil is small compared to its total energy, so that the differential energy loss multiplied by the thickness of the foil gives a good approximation of the total energy deposited by the proton into the foil.

As $E = c\rho VT$, where E is the heat energy contained in an object of constant temperature and c is the specific heat, it follows that $\Delta E = c\rho V\Delta T$ where ΔE is the energy added to the object and ΔT is the associated rise in temperature. This relationship is only approximately correct, as specific heat depends upon the temperature of the object and the temperature rise is assumed to be homogeneous. Considering the energy deposited into an infinitesimal volume element on the foil, ΔE is taken to be dE_{dep} and V to be dV' = dx' dy' t, yielding:

$$\Delta T = \frac{dE_{dep}}{dV'c\rho} = dI'(\frac{dE}{dx})(\frac{t}{cos\theta})\frac{1}{dx'dy'tc\rho} = \frac{I}{2\pi\sigma^2}e^{-(x'^2cos^2\theta+y'^2)/2\sigma^2}dx'dy'cos\theta(\frac{dE}{dx})(\frac{t}{cos\theta})\frac{1}{dx'dy'tc\rho}$$

$$= \frac{I}{2\pi\sigma^2c\rho}(\frac{dE}{dx})e^{-(x'^2cos^2\theta+y'^2)/2\sigma^2}$$

and so an expression for the maximum temperature rise in the foil is found at x' = y' = 0:

$$\Delta T_{max} = \frac{I}{2\pi\sigma^2c\rho}(\frac{dE}{dx})$$

Sudden rises in temperature create thermal stress in materials. As the proton beam pulse passes through the foil in a few micro-seconds, the energy deposition associated with its passage, and hence the temperature rise in the foil, can be assumed to be instantaneous. In this case, the maximum thermal stress in the material can be approximated as:

$$\sigma_{Thmax} = \frac{\alpha_{Th}E_{Young}\Delta T_{max}}{1-\nu}$$

The temperature rise expression has no dependence on the thickness of the foil as the rate of energy deposition $\frac{dE}{dx}$ was assumed to be constant through the foil. The maximum temperature rises of the foil using various materials are listed in Table 1. The temperature rise calculation does not take into account the variation of specific heat with temperature. The proton beam energy is taken to be 40 GeV and the particle beam intensity 3.3×10^{14} protons per pulse.

Temperature Rise in the OTR Detector Foil - MARS Simulation

The MARS15 simulation program was also used to calculate the temperature rise in the foil [6]. The results were fairly close to the calculated values and are summarized in Table 2. The initial temperature of the foil was taken to be 300K and the beam energy 40 GeV.

The results on the MARS simulation depended on the number of events simulated, in cases where there were too few the results could fluctuate by as much as 20 to 40 Kelvin.

Table 1: Temperature Rise in OTR foil - Hand Calculations

	$\Delta T_{max}[K]$ $\sigma_{beam} = 3.5mm$	σ_{Thmax} [MPa] $\sigma_{beam} = 3.5mm$	$\Delta T_{max}[K]$ $\sigma_{beam} = 7.5mm$	σ_{Thmax} [MPa] $\sigma_{beam} = 7.5mm$	σ_{yield} [MPa]
Be	71	335	15	73	240
C(I)	202	41	44	9	80
Ti-6Al-4V	245	388	53	85	900-1170
Ti-$\beta 21s$	193	265	42	58	1277-1373
Ti-15Mo-5Zr	250	360	54	78	920-1330

Table 2: Temperature Rise in OTR foil - MARS Calculations

	$\Delta T_{max}[K]$ $\sigma_{beam} = 7.5mm$	$\sigma_{Thmax}[MPa]$ $\sigma_{beam} = 7.5mm$
Ti	57.94	49.8
C	21.56	0.7
GRPH	35.12	1.1
Be	21.59	70.0

MARS did not provide errors for its temperature rise values. The results are on the same order of magnitude as the hand calculations which indicates that they can only provide a rough estimate of the actual temperature rise.

Temperature Rise in the OTR Detector Foil - FemLab Simulation

Similar temperature rise calculations were carried out in the FemLab finite element solver. This simulation included a more realistic description of the heating and cooling processes acting on the foil. The material parameters used in the simulation to model convective and radiative cooling are included in Appendix 1. The results of the simulation are summarized in Table 3. Four different foil thicknesses are simulated for the Ti-$\beta 21s$ material to demonstrate the dependence of thermal stress on foil thickness.

In this case, T_{rise} is no longer taken to be the maximum rise in temperature that occurs when the beam passes through the foil, but instead is the maximum temperature difference that can exist in the foil at any time. This maximum difference occurs when the foil is operating at the steady state temperature configuration and is slightly larger then the temperature rise induced every time the beam passes through the foil.

The FemLab results are similar in magnitude to the hand calculations which provides some confidence in the validity of both. The titanium alloy and graphite foils are expected to survive in the short term as the stress induced in them is generally much less then the

Table 3: Temperature Rise in OTR foil - FemLab Results

	$\Delta T_{max}[K]$ $\sigma_{beam} = 3.5mm$	σ_{Thmax} [MPa] $\sigma_{beam} = 3.5mm$	ΔT_{max} [K] $\sigma_{beam} = 7.5mm$	σ_{Thmax} [MPa] $\sigma_{beam} = 7.5mm$	σ_{yield} [MPa]	$\sigma_{fatigue}$ [MPa]
Be (10 μ m)	71	335	16	76	240	?
C(I) (10 μ m)	203	41	45	9	80	?
Ti-6Al-4V (10 μ m)	249	395	56	89	900-1170	140-700
Ti-15Mo-5Zr (10 μ m)	258	372	57	82	920-1330	375-700
Ti-$\beta 21s$ (10 μ m)	206	283	48	66	1277-1373	500-800
Ti-$\beta 21s$ (20 μ m)	238	331	-	-	1277-1373	500-800
Ti-$\beta 21s$ (30 μ m)	264	363	-	-	1277-1373	500-800
Ti-$\beta 21s$ (40 μ m)	286	393	-	-	1277-1373	500-800

yield or ultimate strength of the material. However, if a factor of safety of five is required then only the Ti-$\beta 21s$ and Ti-15Mo-5Zr foils can be used. As well, the longterm survivability of the foils depends greatly on the fatigue strength of the material. To ensure the long term survivability of the foils it will be necessary to choose alloys with a suitably high fatigue strength.

Foil Steady State Temperature

The foil is constantly radiating thermal energy for temperatures above the ambient temperature. When the proton beam passes through the foil it deposits extra energy, and so increases the rate at which energy is radiated. The total energy within the foil will decrease until the next pulse passes through. The steady state temperature of the foil is that at which the total energy energy radiated off the foil between pulses is equal to the total amount of energy each pulse deposits in the foil.

Foil steady state temperature can be determined in two ways; by solving the heat transfer partial differential equations with boundary conditions appropriate for a foil, or by hand (by assuming the foil is the same temperature throughout its volume and neglecting thermal conduction and temperature variation). The assumption underpinning the second analysis option is good if the the temperature rise in the foil due to the passage of the proton beam is small compared to the steady state temperature of the foil.

Foil Steady State Temperature - Hand Calculation

The thermal radiation given off by a non-ideal black body of homogeneous temperature is given by $J = \epsilon\sigma_B T^4$ so $P = \frac{dE_{foil}}{dt} = -A\epsilon\sigma_B T^4$ where A is the area of the total radiating surface of the foil [7] (having made the assumption that the foil's temperature is nearly uniform across it's surface). Disc shaped areas will be used in this analysis.

Combining $E = c\rho VT$ and $\frac{dE_{foil}}{dt} = -A\epsilon\sigma_B T^4$, it follows:

$$\frac{dE}{dt} = \frac{-A\epsilon\sigma_B E^4}{(c\rho V)^4}$$

Integrating both sides between the initial and final foil state yields:

$$\int_{Ei}^{Ef} \frac{dE}{E^4} = \frac{-A\epsilon\sigma_B}{(c\rho V)^4} \int_{ti}^{tf} dt$$

$$[\frac{1}{E^3}]_{Ei}^{Ef} = \frac{3A\sigma_B\epsilon}{(c\rho V)^4}(t_f - t_i)$$

The steady state requirement is $E_f = E_i - E_{dep}$, so:

$$\frac{1}{(E_i - E_{dep})^3} - \frac{1}{(E_i)^3} = \frac{3A\sigma_B\epsilon}{(c\rho V)^4}(t_f - t_i) \ ,$$

This last expression is solved numerically, yielding a value of E_i.

The radiating area and volume is given by

$$A = 2\frac{\pi}{cos\theta}(R)^2 \text{ and } V = \frac{\pi R^2 t_{foil}}{cos\theta}$$

R is varied until a limiting temprature rise is found (typically a small value of R)

The next step is to determine what is the energy deposited by the proton beam (E_{dep}). An estimate is found by taking the total energy deposited to be the amount required to raise the temperature of the disc by the maximum temperature rise calculated in the previous section. This is an upper bound to the steady state temperature estimate, as more energy is deposited in the foil then would actually be the case.

$$E_{dep} = c\rho V \Delta T_{max} = V(\frac{dE}{dX})\frac{I}{2\pi\sigma^2}$$

Taking the time between pulses to be approximately 3.53 seconds [2], the steady state temperature can now be calculated. The results for various materials are in Table 4, assuming a 10 μm foil and $\theta = 0$ (material data from [8]):

Table 4: Foil Steady State Temperature - Hand Calculations

	$T_{ss}[K]$ $\sigma_{beam} = 3.5mm$	$T_{ss}[K]$ $\sigma_{beam} = 7.5mm$	$T_{transus}$ [K]
Be	412	263	1500
C(I)	490	274	3800
Ti-6Al-4V	1471	915	1268
Ti-β21s	1459	948	1073
Ti-15Mo-5Zr	1493	956	1000

The steady state temperature is calculated to be high and in some cases greater then the transus temperature. While none of the foils are predicted to melt when the beam is at its normal width, some may melt if the beam is focused down to the 3.5mm for an extended period of time. These hand calculations do not include convective cooling and heat transfer through the foil so they may not provide an accurate description of the steady state temperature.

Foil Steady State Temperature - FemLab Simulation

FemLab can be used to provide an estimate of the steady state temperature by allowing it to simulate the foil experiencing several beam cycles, until it arrives at a repeating temperature distribution cycle (Figure 3). This is the steady state temperature. The results of this simulation are summarized in Table 5.

In this case the steady state temperatures are significantly less then the melting points, and not even much greater than the ambient temperature. This greatly contradicts the hand calculation results. The simulation is more accurate then the hand calculations as

Table 5: Foil Steady State Temperature - FemLab Simulation

	$T_{ss}[K]$ $\sigma_{beam} = 3.5mm$	$T_{transus}$ [K]
Be	372	1500
C(I)	501	3800
Ti-6Al-4V	550	1268
Ti-β21s	504	1073
Ti-15Mo-5Zr	560	1000

Figure 3: Temperature vs. Time for Ti-15Mo-5Zr Heating

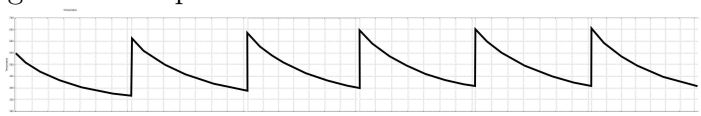

it includes convective cooling and takes the temperature distribution through the foil into account. Both calculations indicate that the foil will not melt under regular beam conditions but differ in whether a sustained over-focused beam will melt the foil. Ideally an over-focused beam will not be allowed to persist long enough to heat the foil to the higher steady state temperature, so it can be concluded that the foil will survive.

Foil Shear Stress

It is interesting to check if the shear stress produced in the foil by the particle beam is sufficient to damage the foil. The force exerted on the foil as a single proton passes through it is given by:

$$\overline{F} = \frac{d}{dt}(m_p \gamma \frac{d\overline{x}}{dt}) = \frac{d\overline{p}}{dt}, \overline{p} = \gamma m_p \overline{v} \text{ [9]}$$

As the proton passes through the foil, it deposits energy and hence loses momentum. Assuming all the lost energy is absorbed by the foil, the force exerted on the foil is proportional to the rate at which the proton is losing momentum. By making the further assumption that the proton loses momentum at a constant rate (similar to assuming that dE/dx is constant), the magnitude of the force exerted on the foil can be approximated as:

$$F \approx \frac{\Delta p}{\Delta t}$$

$$\Delta p = p_f - p_i = \sqrt{\frac{E_f^2}{c^2} - m_p^2 c^2} - \sqrt{\frac{E_i^2}{c^2} - m_p^2 c^2}$$

Using $E_f = E_i - E_{dep}$ and making a few approximations, the total momentum lost by a proton as it passes through the foil is found to be:

$$\Delta p \approx -\frac{E_{dep}}{c} = -\frac{dE}{dx}\frac{t_{foil}}{c}$$

The velocity of a proton of energy E is:

$$v_p = \frac{c^2}{E}\sqrt{\frac{E^2}{c^2} - m_p^2 c^2} = c\sqrt{1 - \frac{1}{\gamma^2}}$$

The proton's velocity is assumed to be constant as it moves through the foil (this assumption is good as the decrease in the velocity is very small compared to the magnitude of the total velocity). The time it takes for the proton to pass through the foil Δt is found to be:

$$\Delta t \approx \frac{t_{foil}}{v}$$

Combining the expressions for the change in momentum and transit time, the force is found to be:

$$F_p \approx \frac{dE}{dx}\sqrt{1 - \frac{1}{\gamma^2}}$$

The shear stress within an object is equal to the magnitude of the force acting on a surface of the object divided by the interior cross-sectional area parallel to the direction of the force and enclosing the surface. In the case of a proton beam passing through a foil, the shear stress along the circumference of a circular surface on the foil (with radius r) is given by:

$$\sigma_{shear} = F_p \frac{I}{2\pi\sigma^2}\frac{1}{2\pi r t_{foil}}(TF)\int\int_{disc} e^{-(x'^2+y'^2)/2\sigma^2} dx'dy'$$

Converting the above integral to polar co-ordinates and solving yields:

$$\sigma_{shear} = F_p \frac{I}{2\pi t_{foil} r}(1 - e^{-r^2/2\sigma^2})(TF)$$

The TF term is the maximum fractional number of protons that are in the foil at any given time. If the proton beam is assumed to be an instantaneous pulse then TF = 1. If the beam is assumed to consist of 9 pulses, each pulse 10 ns in length, then TF is 3.7×10^{-7}

The shear stress was calculated for the three versions of TF described above at different values of r (the distance from the centre of the foil) and the maximum shear stresses found are summarized in Table 6. The maximum shear stress was found to occur at r = 0.012 m when the beam width was 7.5mm and r = 0.006 for 3.5mm.

Table 6: Foil Shear Stress

TF	1	3.7×10^{-7}
	σ_{ss} [MPa]	σ_{ss} [MPa]
Ti-6Al-4V	8.96×10^4	0.03
Ti β-21s	1.06×10^5	0.04
Ti-15Mo-5Zr	1.07×10^5	0.04
C(I)	5.40×10^4	0.02
Be	3.75×10^4	0.01

Shear strength data is more difficult to find then other types, but as a very rough estimate the shear strength of an object can be assumed to be in the same order of magnitude as the tensile strength.

Although these values for the ultimate shear strength are only approximate, it is clear that the two different TF values yield very different results, one in which the foil easily survives and one in which it is always destroyed. The values calculated with TF = 3.71×10^{-7} are the more realistic as they take into account the structure of the proton beam pulse, and so it can be concluded that shear stress failure will not be a problem with the OTR foil.

Thermal Stress and Thermoelastic Waves in the OTR Foil

The T2K beam's passage through the OTR foil will heat it rapidly enough to create a temperature gradient. This temperature gradient creates a body force within the foil and induces thermal stress. Steady state and transient stress distributions are considered.

Steady State Stress Distribution

In the steady state situation with radial symmetry, the relationship between stress (σ_r, σ_θ), strain (ϵ_r, ϵ_θ), the displacement field u_r and a temperature distribution are given by[11]:

$$\sigma_r = \frac{E}{1-\nu^2}[\epsilon_r + \nu\epsilon_\theta - (1+\nu)\alpha T]] \qquad \sigma_\theta = \frac{E}{1-\nu^2}[\epsilon_\theta + \nu\epsilon_r - (1+\nu)\alpha T]]$$

$$\epsilon_r = \frac{\partial u_r}{\partial r} \qquad \epsilon_\theta = \frac{u_r}{r} \qquad T = T(r,t) - T_0$$

$$\frac{\partial}{\partial r}[\frac{1}{r}\frac{\partial}{\partial r}(ru_r)] = (1+\nu)\alpha\frac{\partial T}{\partial r}$$

These equations can be solved directly in the case of a solid circular disk with some radius b (an approximation of the OTR foil) to yield an expression for the steady state stress distributions:

$$\sigma_r = E\alpha[\frac{1}{b^2}\int_0^b Trdr - \frac{1}{r^2}\int_0^r Trdr] \qquad \sigma_\theta = E\alpha[-T + \frac{1}{b^2}\int_0^b Trdr + \frac{1}{r^2}\int_0^r Trdr]$$

There is no true steady state temperature distribution in the OTR foil as the foil will begin to cool directly after being heated by the proton beam. However, the temperature distribution does not change appreciably over time intervals on the order of 1 ms, so for stress distributions considered within these timescales the temperature distribution in the foil can be approximated as:

$$T = T_0 e^{\frac{-r^2}{2\sigma^2}}$$

where T_0 varies between foil materials and beam widths. Calculating the steady state stress with this temperature distribution will yield the stress expected after transient effects die away.

To get the maximum steady state thermal stress induced T_0 is taken to be the maximum temperature difference observed within the foil directly after a proton beam with beam width $\sigma = 3.5mm$ has passed. These temperatures were calculated using FemLab and are summarized in Table 7 along with the calculated maximum thermal stress. An example steady state stress distribution is depicted in Figure 4. The Von Mises stress in a material that experiences plane strain only is given by

$$\sigma_v(r,\theta) = \sqrt{(\sigma_r - \sigma_\theta)^2 + \sigma_r^2 + \sigma_\theta^2}$$

Table 7: Steady State Stress in OTR foil

Material	Foil Thickness [μm]	T_0 [K]	Max. $\sigma_{VMs.s.}$ [MPa]
Ti-β21s	10	206	95
C(I)	10	203	14
Ti-6Al-4V	10	249	126
Ti-15Mo-5Zr	10	258	124

Figure 4: Example Steady State Stress vs. Radial Position

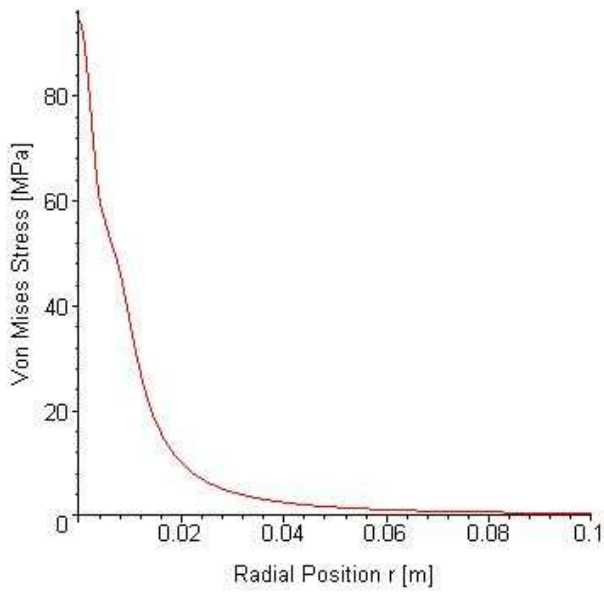

The Von Mises stress criterion states that a material fails when the distortion energy in it equals the strain energy at yield strength for one-dimensional tension. The von Mises stress allows this distortion energy to be compared directly to the yield strength of the material.

<u>Transient Stress Distribution - Thermoelastic Waves</u>

Compressive propagating waves in solids can be created by a thermal gradient. The expression for compressive wave propagation through a solid with radial symmetry is given by [11]:

$$\frac{\partial}{\partial r}[\frac{1}{r}\frac{\partial}{\partial r}(ru_r)] = \frac{1}{c_1^2}\frac{\partial^2 u_r}{\partial t^2} \qquad c_1 = \sqrt{\frac{E(1-\nu)}{(1+\nu)(1-2\nu)\rho}}$$

The expression that couples a thermal gradient to compressive wave propagation is:

$$\frac{\partial}{\partial r}[\frac{1}{r}\frac{\partial}{\partial r}(ru_r)] = (1+\nu)\alpha\frac{\partial T}{\partial r} + \frac{1}{c_1^2}\frac{\partial^2 u_r}{\partial t^2}$$

This equation can be solved numerically for u_r. As the foil is assumed to be unstressed and of uniform temperature before the beam hits, the initial conditions are:

$$u(r, t = 0) = 0 \qquad \frac{\partial^2 u(r,t=0)}{\partial r^2} = 0$$

The edges of the foil are assumed to be fixed, and by symmetry the displacement at r = 0 must always be zero, yielding the following boundary conditions:

$$u(r = 0, t) = 0 \qquad u(r = b, t) = 0$$

The foil radius b was assumed to be 3cm in the simulations.

The temperature distribution is assumed to be approximately gaussian in r and of the same standard width of the particle beam (taken here to be 3.5mm). The temperature increases linearly as the beam pulse passes through and then remains roughly constant over the timescales in which wave propagation through the foil occurs. The temperature distribution can be expressed as:

$$T = T_0 \tanh(\tfrac{2t}{5\times10^{-6}})e^{-r^2/2\sigma^2}$$

where T_0 is the maximum temperature that occurs in the foil. When only considering stress waves produced during beam heating, the temperature expression becomes:

$$T = T_0(\tfrac{t}{5\times10^{-6}})e^{-r^2/2\sigma^2}$$

The stress distribution can now be solved numerically for any time. The maximum Von Mises stress that occurs in the center of the foil for each material is summarized in Table 8, which also includes the T_0 value that specifies the temperature distribution for that material. It is found that the maximum stress at the foil center is approximately given by:

$$\sigma_{vm}(r = 0) = \tfrac{\alpha E T}{1-\nu}$$

This is the same formula used in the temperature rise section to deduce the stress induced by the temperature change.

Table 8: Transient Stress in OTR foil

Material	Foil Thickness [μm]	T_0 [K]	Max. $\sigma_{VM}(r = 0)$ [MPa]	σ_{yield} [MPa]
Ti-β21s	10	206	283	1277-1373
C(I)	10	203	41	80
Ti-6Al-4V	10	249	382	900-1170
Ti-15Mo-5Zr	10	258	371	920-1330
Be	10	71	335	240

<u>Stress Calculations - Conclusion</u>

The dynamic and steady state stress of the OTR composed of various materials has been calculated and a large degree of agreement has been found between the various results. The dynamic stress induced in the OTR foil is likely to be on the same order of magnitude as those in Table 6. A titanium alloy or graphite foil is expected to survive the T2K beam in the short term, however long term survivability will depend on the fatigue strength of the material that is eventually chosen. The effect of shock waves has not been considered but should be in future as they may cause the foils to fail sooner then expected.

Radiative Heating of OTR Foil by T2K Target

The target station OTR detector is to be placed between the proton-beam target and collimator. The target is estimated to approach a steady-state temperature distribution of 673 K at the centre down to 573 K at a radial distance of 15 mm. The radiative and convective heating effect of the target on the steady-state temperature of the OTR foil is investigated.

Radiative Heating - Estimate

A crude upper-estimate of the temperature rise of the OTR foil due to radiative heating can be made by assuming the OTR foil is directly facing the target, that the target is uniformly 673 K but diffusely emits all thermal radiation from a point at its centre, and that the radiation incident on the foil heats it uniformly. Additionally take the foil to be a disc of variable radius and the ambient temperature to be 300 K.

The fractional amount of power radiated from the target that hits the foil is given by:

$$F = \frac{\int_0^{2\pi} d\phi \int_0^{\theta_f} d\theta R^2 \sin(\theta_f)}{2\pi R^2} = (1 - \cos\theta_f)/2$$

with $\theta_f = \tan^{-1}(r_{foil}/distance)$

The average power radiated onto the foil can be estimated as:

$$P = \sigma_B \epsilon (T_{amb}^4 - T^4) \pi r_{target}^2 (1 - \cos\theta_f)/2$$

The average heat flux is:

$$q = \frac{P}{\pi r_{foil}^2}$$

The temperature rise in the foil over time (Δt) is estimated as

$$\Delta T = \frac{P\Delta t}{c\rho V_{foil}} = \frac{P\Delta t}{c\rho\pi r_{foil}^2 t_{foil}}$$

where c is the material's specific heat, ρ the density, V_{foil} the foil's volume and t_{foil} the foil's thickness.

Using a 10 μm thick foil of Ti-6Al-4V ($\epsilon = 0.01$), the temperature rise is calculated for foils with different radii. The temperature rise is found to approach an asymptotic value as the radius of the foil is decreased indicating that the center of the foil is heated most as expected. The asymptotic temperature rise rate is found to be $\Delta T = 0.67\epsilon[K/sec]$. This upper bound estimate is a relatively small temperature rise compared to the temperature rise due to the passage of the beam pulse.

This analysis shows that radiative heating from the target to the foil is not expected to be a significant factor.

Figure 5: OTR Angular Distribution

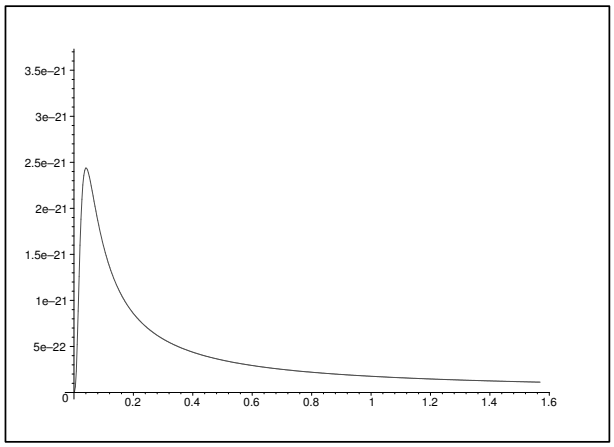

Optical Transition Radiation

Radiation is emitted whenever a charged particle crosses an interface between two mediums with different dielectric constants. This radiation has a distinctive angular and frequency distribution that is described by the formula [12]:

$$\frac{d^2I}{d\nu d\eta} = \frac{z^2\gamma\hbar\alpha\omega_p}{\pi}\frac{\eta}{\nu^4(1+1/\nu^2+\eta)^2(1+\eta)^2}[J/rad^2]$$

$$\nu = \text{dimensionless frequency variable} = \frac{\omega}{\gamma\omega_p}$$

$$\eta = (\gamma\theta)^2$$

$$\omega_p = \text{plasma frequncy} = \frac{NZe^2}{\epsilon_0 m_e}$$

NZ is the number of electrons per unit volume of the dielectric, ω is frequency and θ is the polar angle.

It is worthwhile to plot the energy distribution in terms of the polar angle θ. This is done by first integrating over visible frequencies, then integrating the distribution over a small angular range and plotting the resultant energy against the center of that angular range. If the angular ranges are made small enough the plot will resemble the $dI/d\theta$ curve. This is shown in Figure 5.

This curve can be approximated by the simplified expression

$$\frac{dI}{d\theta} = C \times 10^{-22}\frac{\theta^2\sin\theta}{(\gamma^{-2}+\theta^2)^2}$$

with C some constant, which is plotted in Figure 6.

Figure 6: OTR Angular Distribution - Simplified Expression

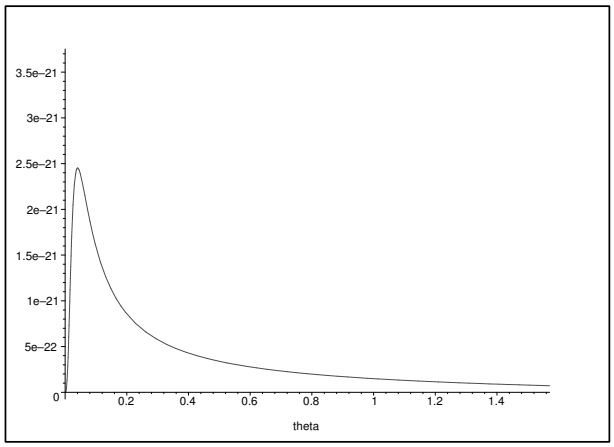

As can be seen these two curves are very similar in shape, though the second curve has a much simpler dependence on θ. This second curve will be the one used in the optical simulation when trying to determine the amount of energy radiated into a solid angle.

Optical Simulations

Optical simulations are necessary to determine if the optical system design is feasible. An optical simulation program was written to simulate how light would move through the optical system and predict the final image. This simulation was applied to the OTR optical system in order to evaluate the quality of the image produced and whether it met the minimum requirements. The program was also used to specify the width of the channel that allows light to pass through the optical system.

The optical simulation program consisted of a ray tracing routine and a loop that defined the initial rays in an appropriate way and accumulate the amount of light deposited on the image plane by incident rays.

Ray Tracing

The ray tracing routine accepts an initial ray (to be defined below) and traces it through a representation of an optical system. The ray either successfully traverses the optical system and contributes to the image or it doesn't and the routine ends. The basic elements of the ray tracing program are a co-ordinate system, the rays, the reflective surfaces and cutoffs.

The three dimensional spatial co-ordinate system origin is positioned at the focal point of the first parabolic mirror in the system. A diagram showing the co-ordinate system and the orientation of the optical system and beam direction within it is in Figure 7.

Figure 7: Global Co-ordinate System

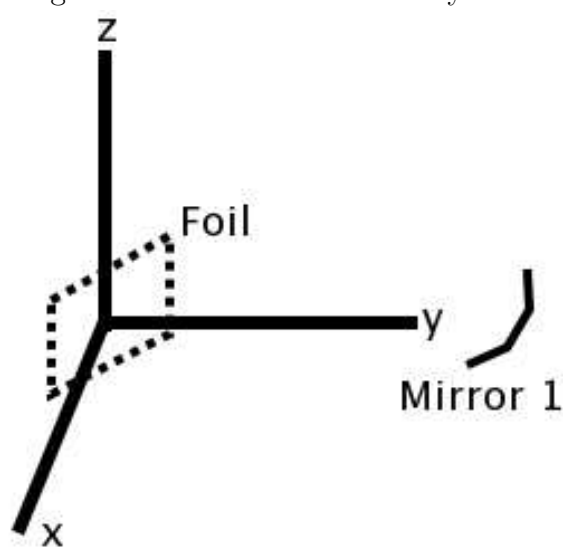

A ray is defined as a straight line parameterized in the co-ordinate system. It consists of a vector and the point from which it is emitted. Each ray has a weight that is determined by the angular distribution of the radiation source. Diffuse light sources require each ray to have the same weight, while weights for optical transition radiation depend on the polar angle of the ray relative to the specular reflection axis of the foil.

Cutoffs are restrictions on the regions of space through which rays can travel and are implemented with if statements. They are used to define the light pipe and mirror boundaries.

Reflective surfaces are represented as two-dimensional functions of the co-ordinate system, ie.

$$z = f(x, y)$$

Most of surfaces in this program are parabolic mirrors, but other types of shapes can be used. Each surface shape has a boundary that is implemented using a cutoff. The surfaces are ordered in a sequence so that as the ray proceeds through the system it will hit each surface in order. The first surface in the sequence is the 1st mirror, the last surface is the image plane.

The ray tracing routine's operation has three steps which are summarized below.

1. Define the ray and the next surface in the sequence.

2. Determine if the ray intersects the next surface in the sequence, or if it hits a cutoff. If the ray hits a cutoff the routine terminates without changing the image plane.

3. If the ray hits the next surface and the surface is not the image plane, a reflected ray is defined and the routine returns to step 1 one increment further in the surface sequence. If the ray intercepts the image plane, the ray's weight is added to the appropriate bin in the image plane array and the routine finishes.

The routine must determine the intersection point of a ray and surface in step 2. The routine does this using Newton's method to find the solution to the series of equations describing the ray and surfaces:

$$x_R(t) = V_x t + I_x$$

$$y_R(t) = V_y t + I_y$$

$$z_R(t) = V_z t + I_z$$

$$z_S = f(x, y)$$

Specifically, the value of t must be found for which $z_R = z_S$. This is equivalent to finding the root of the function

$$F(t) = z_R(t) - f(x_R(t), y_R(t))$$

Newton's method is an iterative process that finds better and better approximations of the intersection point with the sequence:

$$t_{n+1} = t_n - \frac{F(t_n)}{F'(t_n}$$

The only requirement for Newton's method to work is that the derivative of the function be well defined and the initial element of the sequence t_0 be sufficiently close to the actual intersection point.

In step 3 the reflected ray must be calculated after the ray intersects a mirror surface. The reflected vector is found by decomposing the original vector into the components that are parallel and perpendicular to the normal vector of the surface at the point the ray is incident, then taking the vectorial sum of the original perpendicular component and the negative of the parallel component. The formula for the surface normal vector is given below for a surface defined in the form of $S(x, y, z) = 0$:

$$\hat{n} = \frac{\nabla S}{\sqrt{S_x^2 + S_y^2 + S_z^2}}$$

while the formula for the reflected vector is

$$\overline{V}_R = \overline{V}_i - 2(\overline{V}_i \cdot \hat{n})\hat{n}$$

Optical System Simulation

The ray tracing algorithm is part of the total optical system simulation that includes information about the proton beam shape and intensity, OTR foil orientation and the angular distribution for transition radiation. The simulation is used to produce images that approximate the output of the real system and to compare different possible system configurations through the simulated output. The quality of the system can be evaluated from simulations measuring the amount of light lost by the system, relative light acceptance from different parts of the foil and the overall distortion and bluriness the system introduces into beam images.

The main elements of the system consist of the ray tracer, a foil parametrized as a plane in the co-ordinate system, a beam intensity distribution parameterized in the co-ordinate system and the image plane array. The program procedure is as follows.

1. The program divides the foil plane into foil elements with each element centered at a particular co-ordinate.

2. The program loops through each foil element (co-ordinates), dividing the solid angle centered about the foil specular reflection axis into solid angle elements. The program loops through each solid angle element.

3. For each foil/solid angle element the program defines a ray with an appropriate initial position, vector and weight. This ray is then passed on to the ray tracer.

4. If the ray tracer finds the ray is incident on the image plane, the ray's weight is added to the appropriate bin on the image plane array.

5. After looping through all foil/solid angle elements the image plane array is written to file, it is now the simulated beam image.

In the case of optical transition radiation the ray vector's weight is determined by both its angle relative to the specular reflection axis and by its position on the foil. The angular dependence is determined directly from the OTR angular distribution, though an approximation is made by assuming the angular distribution does not change significantly over the solid angle element associated with the ray. This allows the angular contribution to the weight to be determined directly from the angle and solid angle element area using the formula:

$$\Delta U = \frac{1.713\times10^{-22}}{2\pi}\frac{\theta^2\sin\theta}{(\gamma^{-2}+\theta^2)^2}\Delta\theta\Delta\phi$$

The beam intensity distribution affects the ray weight as well through the foil element position. The proton beam intensity distribution is taken to be gaussian in the plane transverse to the beam direction, and this plane is projected onto the foil plane surface. The projected distribution onto the foil plane is what affects the weight.

One use of the optical simulation is to estimate the size of the light pipe needed at various points along the optical path. These sizes are summarized in Figure 2 for the current system design.

Simulation Results

The optical simulation was applied to the system configuration described in the System Design section.

The distortion the optical system introduces into beam images can be seen by simulating the image created by a grid of point sources placed on the foil. The results of this simulation are shown in Figure 8, where the distortion effect is obvious.

This simulation also allows the relative light acceptance for different points on the foil to be

Figure 8: Image of Grid of Point Sources

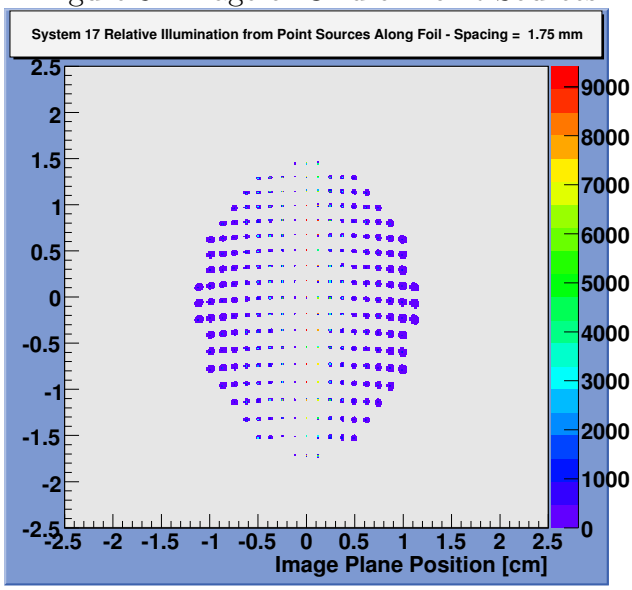

measured. The system response to light emitted from different parts of the foil must be as uniform as possible in order to correctly deduce the beam shape from the image. The results of this measurement are shown in Figure 9 and it can be seen that relative light acceptance never varies more then 10 % from the maximum value.

The blurriness induced by the optical system can be estimated by calculating the width of a point source's image on the image plane. The results of this are shown in Figure 10 and 11, and demonstrate a regular increase in blurriness for points further away from the center of the foil. The maximum RMS spread of a point's image in the viewable are is 0.2mm, which is small compared to the beam widths to be imaged. For this reason image blurriness is not expected to prevent the beam width from being measured accurately.

The optical simulation can be used to simulate actual beam images. An example of this is in Figure 12 for a Gaussian beam with 7.5mm standard width. This type of simulation allowed the amount of light incident on the image plane to be calculated as 0.5×10^{-14} W for the period the beam is passing through the foil.

All of these optical simulations indicated that the proposed system was expected to provide the required beam position and width resolution while having a uniform light acceptance and minor blurriness. At this point a prototype optical system was constructed to test these optical simulations as well as to further investigate the feasibility of this system.

Figure 9: Percentage Light Acceptance for Different Points on Foil

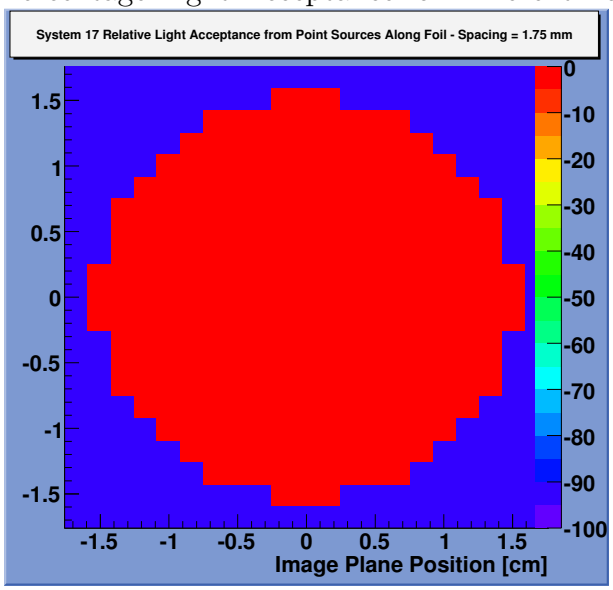

Figure 10: Horizontal RMS Width of Point Source Images

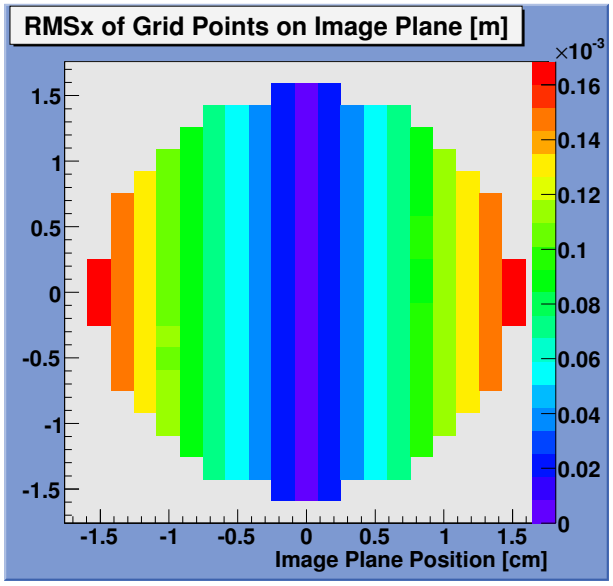

Figure 11: Vertical RMS Width of Point Source Images

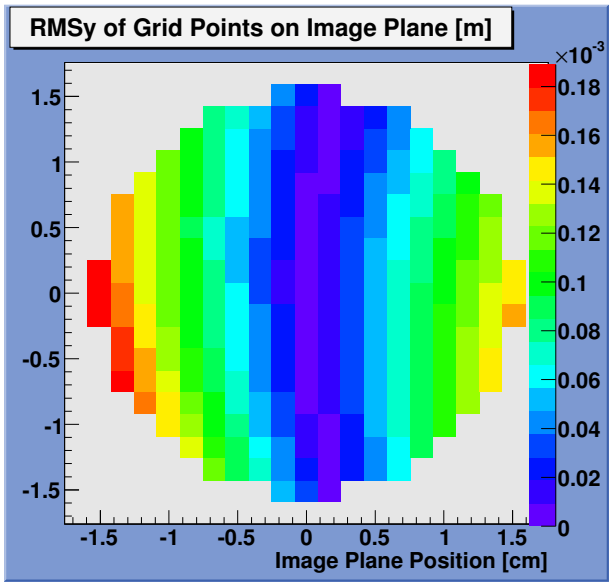

Figure 12: OTR Simulated Beam Image

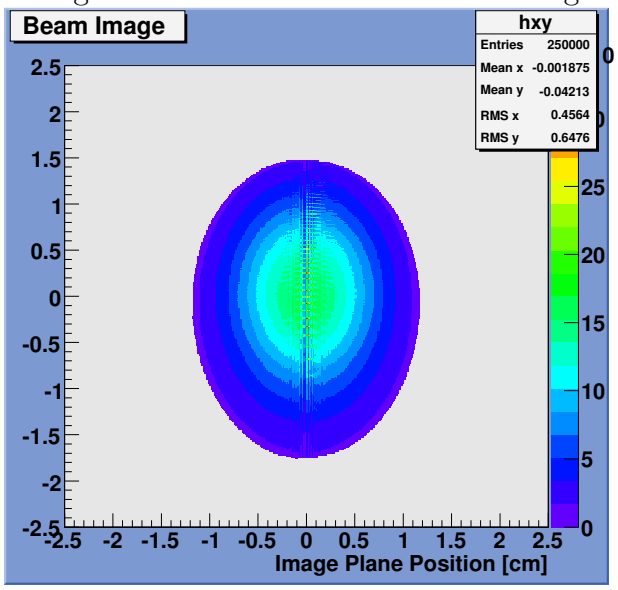

Figure 13: Prototype Optical System

OTR Detector Prototype Test

The Prototype

The prototype OTR optical detector is a scaled down version of the full optical system design. It is implemented on an optical table with standard optical components (Figure 13). The prototype was constructed in order to verify the simulations of the optical response as well as to determine if the optical system could observe OTR light and beam shapes.

Initial Prototype Tests

The first test of the prototype optical system was to determine if it could produce a clear image of an object placed at the focal point. For this test a snowflake image was chosen, and as seen in Figure 14 it was successfully imaged by the system. A distinctive distortion in the image can be observed, which is an unavoidable consequence of using parabolic mirrors.

A more advanced test was to see if the prototype images corresponded to the images produced in simulations. A piece of graph paper was imaged and the grid vertex positions were compared to a simulated image of a grid of point sources with the same spacing as the graph paper. The two sets of points are plotted in Figure 15 and the simulation is found to correctly predict the distortion introduced by the optical system. This confirmation meant the system worked well enough to proceed to the next stage in testing.

Prototype NRC Test

Figure 14: Prototype Test Image

Figure 15: Graph Paper Grid vs. Simulated Grid

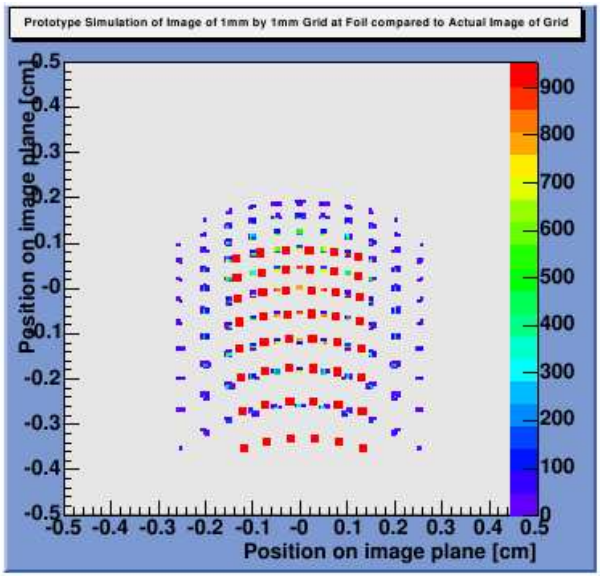

Figure 16: Raw Beam Image

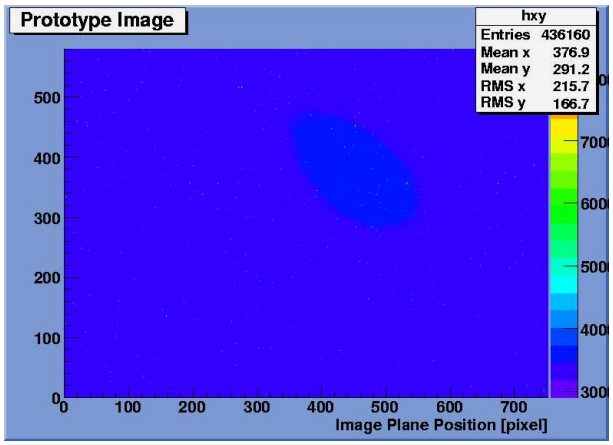

The purpose of the NRC test was to determine if the system could detect OTR light, whether it could image the beam shape from the OTR light and if changes in the beam's position and shape could be observed. Finally, the observations of the beam's width and change in position are compared to the NRC wire monitor detector's measurements to test the accuracy of the OTR system.

Beam Images

Optical transition radiation was detected during the NRC beam test and several dozen images of the NRC beam were recorded. An example 'raw' image is shown in Figure 16. The beam shape is not readily observed in the image due to the presence of 'hot' pixels in the camera that distort the scale used when displaying the image. These pixels can be found by taking a dark image (an image when the camera aperture is covered), which is also used to determine the magnitude of signal noise created by the camera itself. The dark image used in this analysis is shown in Figure 17.

The beam images are distorted by the parabolic mirrors used in the detector's optical system. This distortion can be corrected by applying a transformation to the image, though this transformation requires multiple fiducial markings to be well defined. The images taken during the NRC test do not have enough fiducial holes visible in order to define a useful transformation. Instead a general transformation is defined using simulated images of fiducial holes. Although this transformation is only valid for an ideal system with perfect alignment, it can be applied to the images taken with the real system to obtain a better approximation of the undistorted beam image.

Figure 17: Dark Image

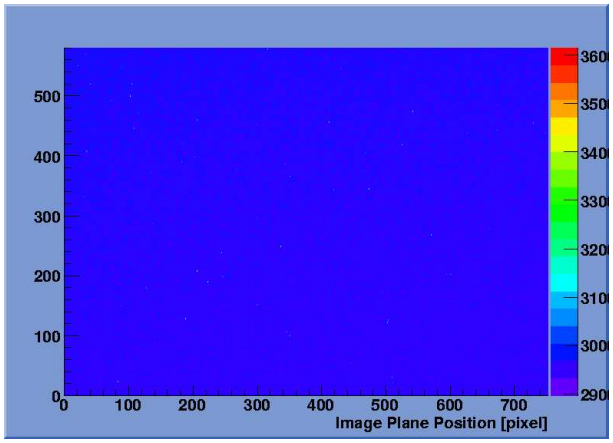

Beam Fits

Fits were applied to the beam images in ROOT. The following two dimensional Gaussian function was applied to the NRC beam images:

$$Ae^{-r_1^2/2B^2 - r_2^2/2C^2} + D$$

$$r_1 = \cos(E)(x - F) + \sin(E)(y - G)$$

$$r_2 = -\sin(E)(x - F) + \cos(E)(y - G)$$

The constant term takes into account the background noise produced by the camera and uniform ambient light. A flat distribution of the following form was used to fit dark or beam off images:

$$Ax + By + C$$

Comparison Between Methods

When analyzing the beam shape there are several options available to deal with hot pixels:

a) Do nothing as the beam fits will not be seriously altered by outliers.

b) Subtract the dark image out from the images.

c) Replace pixels whose value are greater then some multiple of the average value of adjacent pixels with the average value.

Figure 18: Dark Image Subtracted

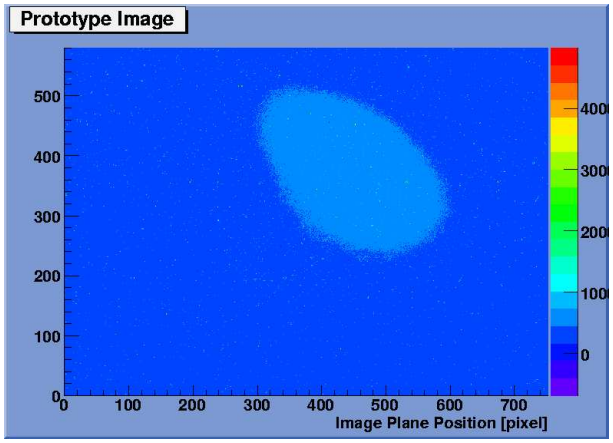

d) Fit the dark image to some function then subtract the fit from the images.

An example of the image produced by each method are in Figures 16,18,19 and 20 respectively. The method that produces an image with the lowest χ^2 value when fitted is the best. Such fits were made and the results are presented in Table 10.

The various methods produce results that differ by more then the calculated error. The

Table 9: Fits for Various Background Removal Methods

Method	A	B	C	D	E	F	χ^2
a	321.0	443.5	106.6	367.6	105.9	2948.2	426659
b	307.1	432.2	111.2	349.9	110.8	4.62	6.9×10^6
c	321.0	443.5	106.5	367.4	105.8	2946.4	131651
d	310	431.4	113.6	345.8	110.2	1.084	7.5×10^6

χ^2 test indicates that the fits are better when the dark image information is not used, and removing the hot pixels does not significantly change the fit results. The unaltered images will be used when analyzing the beam widths and position shifts. However, the discrepancy between the fit results for the different methods must be explained.

Beam Widths and Position Shifts

Changes in the beam position and width were directly observed during the test, as is shown in Figure 21. Gaussian fits were applied to the beam steering test images to determine

Figure 19: Smoothed Image

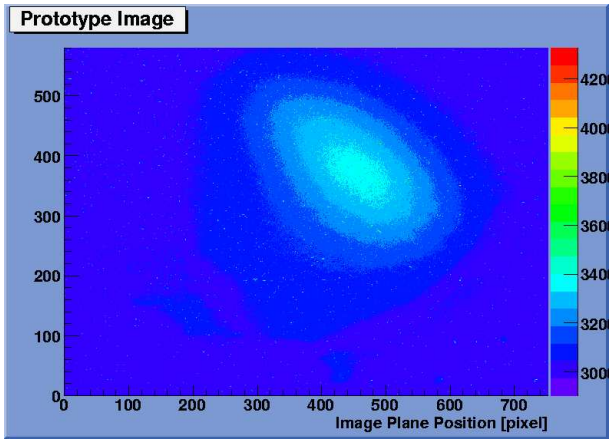

Figure 20: Dark Image Fit Subtracted

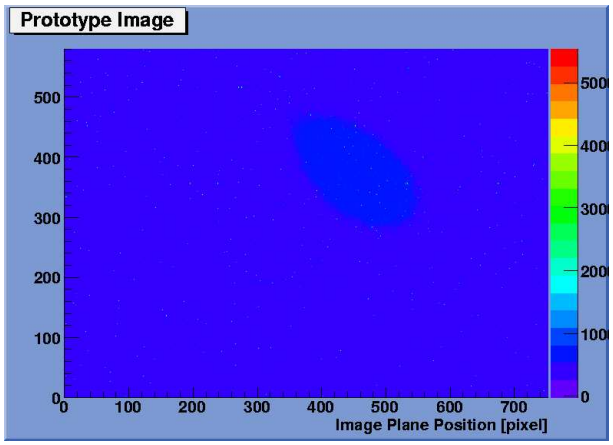

Figure 21: Beam Position Change

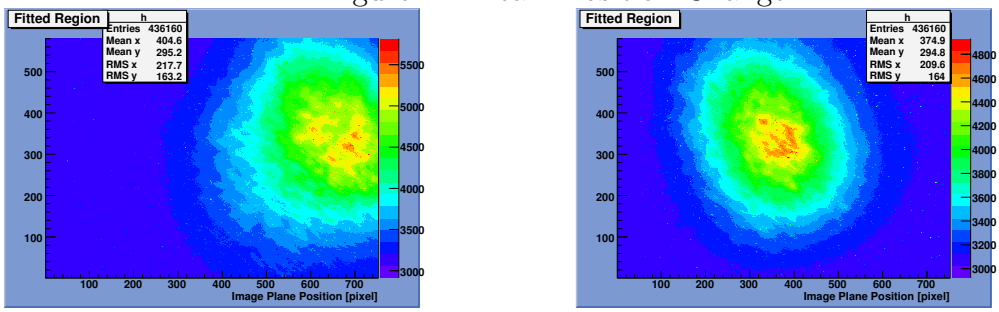

Figure 22: NRC Wire Chamber Monitor Output

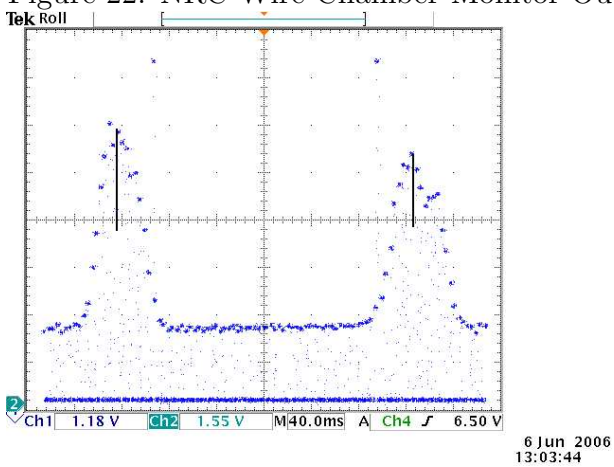

how closely the beam width and position changes observed in the images matches the beam width and position shifts as measured by the NRC beam profile monitor. The beam width at the OTR detector foil is expected to be wider then at the NRC monitor due to multiple scattering events in the air and beam window. The results of the fits for various images are summarized in Table 10. The width of the beam at the foil are deduced from these fits and are summarized in Table 11.

An example of the NRC wire chamber beam monitor output is shown in Figure 22, with one half corresponding to the horizontal position and the other the vertical position. Markings are included to label the position of the center of each peak. The beam position is taken to be at the center of each peak. The beam width is estimated by measuring the full-width half-maximum of the peak which can be related to the beam sigma (assuming a Gaussian beam).

Table 10: Beam Image Fits

Image	Material	Amp.	σ_1	σ_2	Noise	Angle [rad]	x-pos	y-pos
57	Ti	413	98.7	152.0	2963	0.37	534.2	450.9
58	Ti	300	99.7	151.5	2957	0.35	460.7	405.8
59	Ti	423	99.1	164.9	2970	0.26	525.8	537.9
61	Ti	360	98.9	143.1	2958	0.42	519.3	362.9
90	Graphite	37.9	103.5	158.6	2933	0.52	357.0	306.7
92	Graphite	51.8	121.6	164.5	2938	0.71	674.3	292.8
94	Al	1547	142.6	151.0	2972	0.01	523.9	481.5
95	Al	1951	155.6	151.8	2966	-0.57	661.8	343.7
96	Al	1422	140.4	105.3	2970	1.97	354.2	345.0
Dark Image	na	-0.0533	0.006	2969.4				

Table 11: Beam Widths

Image	Material	OTR σ_1 [mm]	OTR σ_2 [mm]	OTR σ [mm]	Wire at foil σ_x [mm]	Wire at foil σ_x [mm]	Wire at foil σ [mm]
57	Ti	1.15	1.70	2.05	1.62	1.76	2.39
58	Ti	1.16	1.70	2.05	1.63	1.83	2.45
59	Ti	1.15	1.85	2.18	1.64	1.77	2.42
61	Ti	1.15	1.60	1.97	1.74	1.80	2.51
90	Graphite	1.20	1.78	2.14	1.69	1.81	2.48
92	Graphite	1.41	1.84	2.32	1.67	1.80	2.45
94	Al	1.65	1.69	2.37	1.73	1.84	2.53
95	Al	1.81	1.70	2.48	1.74	1.83	2.53
96	Al	1.63	1.18	2.01	1.76	1.79	2.51

The titanium foil beam images have an average beam sigma of 2.06 $\pm$0.08 mm, the graphite images have 2.23 $\pm$0.13 mm and the aluminum images 2.29 $\pm$0.25 mm. Although these measurements are consistent, the beam images taken with the titanium foil are more oval in shape than those taken with the other foils. It is possible that warping of the titanium foil is changing the observed beam shape, though this can't be known for sure. The beam width for the aluminum foil corresponds to a full-width half-maximum of 2.70 $\pm$0.02 mm.

When the electron beam passes through the air, it widens due to multiple coulomb scattering in the foil. Assuming a γ of 40 and a flight distance of 2 cm in air, the RMS square deflection of the beam is found to be 1.35mm. This distance is added in quadrature with the

wire monitor beam width data to determine the expected beam widths at the foil, which are included in Table 11. The wire monitor measurements agree with the OTR measurements for some foils better then others, with the greatest disagreement in the case of the titanium foil.

The observed beam position shifts are compared to the wire monitor output in table 12. The observed shifts do not correspond precisely in magnitude to the shifts detected by the wire monitor but are consistent within roughly 0.35mm, which is better then the required position resolution of 1mm. Bean widths measured by the two detectors agree on average within 12%.

Table 12: Beam Position Shifts

Image	Material	x-pos. [mm]	y-pos. [mm]	Shift [mm]	Monitor x [mm]	Monitor y [mm]	Monitor Shift [mm]
57	Ti	6.20	5.05	0.0	6.0	7.3	0.0
58	Ti	5.34	4.54	0.99	5.0	7.0	1.0
59	Ti	6.10	6.02	0.98	5.5	6.3	1.1
61	Ti	6.02	4.06	1.00	7.0	6.3	1.4
90	Graphite	4.14	3.43	0.0	8.0	7.8	0.0
92	Graphite	7.82	3.28	3.68	8.0	3.8	4.0
94	Al	6.08	5.39	0.0	6.0	5.5	0.0
95	Al	7.68	3.85	2.22	7.8	4.0	2.3
96	Al	4.11	3.86	2.49	7.8	8.0	3.1

Reflectivity Comparison

Different foils composed of different materials were used during the NRC test. It is interesting to determine if there is any relationship between the foil material's reflectivity and the intensity of OTR light produced. To make this comparison, OTR images were taken with different foils and the electron beam located in roughly the same place and at the same intensity. Gaussian fits were applied to the resulting images in order to deduce the Gaussian amplitude parameter which can be used as a measure of the OTR light intensity (see Gaussian fit formula). The results are summarized in Table 13.

There does not seem to be a precise relationship between material reflectivity and the beam image intensity. The magnitude of the A parameter seems to vary significantly even for the same foil material, so this comparison may not be conclusive. The reason for the variation may be due to the fact that many of the images were taken when the beam was outside the viewable area the system was designed for. The size of the viewable area is shown

Table 13: Foil Reflectivity

Image	Foil Material	Amp.	Reflectivity
58	Ti-alloy	300	0.4 - 0.5
96	Al	1422	0.9
90	Graphite	37.9	0.1 - 0.2

Figure 23: Viewable Area

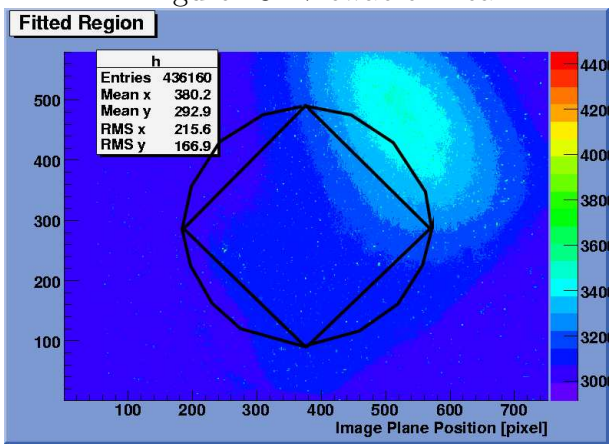

in Figure 23. Outside the viewable area the light acceptance is not uniform across the foil which may cause the image of the beam shape to be distorted.

Origins of Noise

There are three sources of noise in the beam images; the camera, ambient light, and light produced by the beam's interaction with matter that is not OTR light. Fits were performed on all the dark and beam-off images using the formula $Ax + By + C$ with the results summarized in Table 14.

The dark image (Figure 17) gives an estimate of the dark noise inherent to the camera, and the fit performed on this image indicates a constant 2925 value in each pixel can be ascribed to noise. In addition there is a static-like noise such that each pixel deviates from this constant, though the RMS deviation of all the pixels from the fit show that this type of noise is small compared to the magnitude of the signal and constant noise term. What is not small in comparison to this constant noise are hot pixels, though methods of dealing with them have been mentioned already. Finally there is the variation of the constant noise

term with the position on the image (the x and y slopes) though the fits show that this is very small.

The effect of ambient light and non-OTR light produced by beam interaction can be seen by comparing the dark image fit constant term to the constant terms found in beam image fits. Any increase in the constant term is presumably due to these other noise sources. As can be seen in Table 14, the constant term can vary widely, the most likely explanation being the effect of ambient light noise. However, some of the fits can have constant terms very close to the dark image current, indicating that it is possible to eliminate most of the ambient light.

It seems clear that noise for the OTR detector can be modeled as a constant value added to each pixel and can be included in the fits.

Table 14: Dark Images and Noise

Image	Constant	x-slope	y-slope	RMS dev.
Beam off 31	4694.03	0.06	-0.03	35.49
Beam off 43	2969.44	-0.05	0.01	14.75
Beam off 131	2938.34	0.00	0.01	8.66
Dark Image	2924.75	0.00	0.01	7.47

Helium Bag Test

The prototype optical system was enclosed in a plastic bag which was flushed with helium gas. Beam images were taken to check if Cherenkov light would be a problem in a helium gas environment. The amount of helium gas present was not measured, however a large volume of gas was allowed to flow through the apparatus before measurements were made so it is assumed that it was the proportion of helium in the air was elevated. Initially there seemed to be no evidence of Cherenkov light as a regular beam image is obtained, see Figure 24. However, when the beam was deflected away from the foil by a magnet light could still be seen (Figure 25). Further experimentation demonstrated that the light that was observed was actually transition radiation emitted off of the beam window. When this was corrected for no evidence of Cherenkov light was found in the elevated helium environment.

Figure 24: Helium Test Example Image

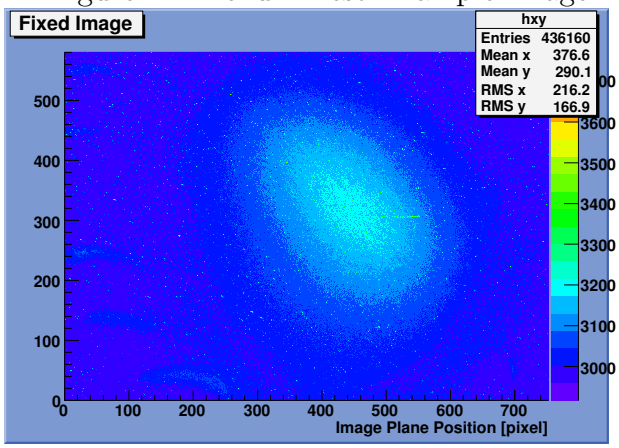

Figure 25: Image with Electron Beam Deflected

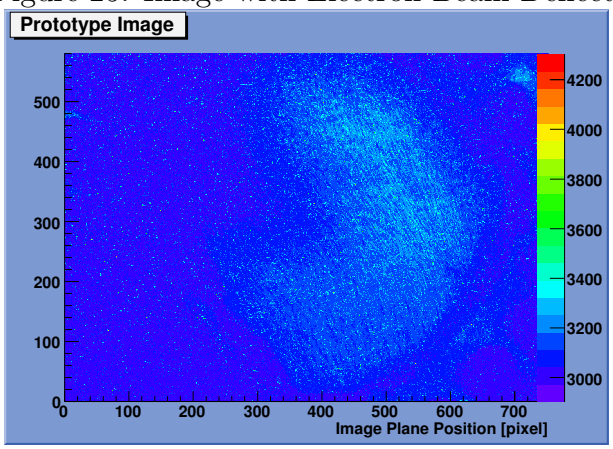

Conclusion

A beam monitor is required to detect the T2K proton beam width immediately before it hits the production target. The Optical Transition Radiation detector design presented in this report has been shown to be able to survive the thermal damage caused by the proton beam's passage and optical simulations have demonstrated that it can image the beam and has suitably uniform light acceptance across the foil surface (less then 10 % variation). A prototype was constructed and tested in the NRC electron beam and OTR light was detected and beam images observed. The success of the NRC test demonstrates that the OTR detector design presented in this report can be used as the proton beam monitor in the T2K target station.

References

/[1] V. Scarpine et al., "Test of an Optical Transition Radiation Detector for High-Intensity Proton Beams at FNAL". 2003 IEEE Nuclear Science Symposium (2003)

/[MNS] Z. Maki, M. Nakagawa, S. Sakata, Prog. Theor. Phys. 28, 870 (1962)

/[2] "T2K Letter of Intent", hep-ex/0106019 (2003)

/[3] W.R. Leo, "Techniques for Nuclear and Particle Physics Experiments" (Springer-Verlag New York, Inc, 1996)

/[4] P. Sievers, "Thermal Stress and Thermo-Acoustic Waves Implications for Choice of Material" (Collimation Day 2002)

/[5] R.M. Sternheimer, M.J. Berger and S.M. Seltzer, Atomic Data and Nuclear Data Tables 30, 261-271 (1984).

/[6] N.V. Mokhov, "The Mars Code System User's Guide", Fermilab-FN-628 (1995);
O.E. Krivosheev, N.V. Mokhov, "MARS Code Status", Proc. Monte Carlo 2000 Conf, p. 943, Lisbon, October 23-26, 2000; Fermilab-Conf-00/181 (2000);
N.V. Mokhov, "Status of MARS Code", Fermilab-Conf-03/053 (2003);
N.V. Mokhov, K.K. Gudima, C.C. James et al, "Recent Enhancements to the MARS15 Code", Fermilab-Conf-04/053 (2004);
http://www-ap.fnal.gov/MARS/.

Neither the name of URA/Fermilab nor the names of its contributors may be used to endorse or promote products derived from this software without specific prior written permission.

/[7] C. Kittel, H. Kroemer, "Thermal Physics" (New York W.H. Freeman and Company,

1980)

/[8] MatWeb, Material Property Data, www.matweb.com

/[9] A.O. Barut, "Electrodynamics and Classical Theory of Fields and Particles" (New York Dover Publications Inc. 1980)

/[10] Sadd, "Elasticity" (Amsterdam ; Boston : Elsevier Butterworth Heinemann, c2005.)

/[11] Timoshenko and Goodier, "Theory of Elasticity" (New York : McGraw-Hill, [1969, c1970])

/[12] J.D. Jackson, "Classical electrodynamics" (New York : Wiley, c1999.)

Appendix 1 - OTR Foil Materials Summary

The OTR detector foil will experience rapid heating during proton beam operation that will induce a significant amount of thermal stress. It is necessary to insure that the foil will survive this stress over a long period of beam operation as replacing the foil would require extensive work. For these reasons the choice of foil material is important. The materials used in this analysis and their relevant properties are included in the table below (values from Sternheimer et al. [5], also PDG). These parameters are used to calculate the energy

Table 15: Material parameters used to calculate dE/dx

	$\rho[kg/m^3]$	Z	A	$I[eV]$	X_0	X_1	δ_0	C	a	K
Ti	4540	22	47.9000	233	0.0957	3.0386	0.12	4.4450	0.15660	3.0302
Al	2699	13	26.9815	166	0.1708	3.0127	0.12	4.2395	0.08024	3.6345
V	6111	23	50.9420	245	0.0691	3.0322	0.14	4.2659	0.15436	3.0163
Be	1848	4	9.0122	63.7	0.0592	1.6922	0.14	2.7847	0.80392	2.4339
C(I)	2265	6	12.01115	78	-0.0178	2.3415	0.12	2.8680	0.26142	2.8697
Fe	7874	26	55.8450	286	-0.0012	3.1531	0.12	4.2910	0.14680	2.9632
Si	2329	24	28.0855	173	0.2015	2.8716	0.14	4.4355	0.14921	3.2546
Zr	6506	40	91.2240	393	0.2957	3.4890	0.14	5.1774	0.07177	3.4533
Sn	7310	50	118.7100	488	0.2879	3.2959	0.14	5.5340	0.18689	2.8576
Mo	10220	42	95.9400	424	0.2267	3.2784	0.14	4.8793	0.10525	3.2549
Nb	8570	41	92.90638	417	0.1785	3.2201	0.14	5.0141	0.13883	3.0930
Cr	7180	24	51.9961	257	0.0340	3.0451	0.14	4.1781	0.15419	2.9896

deposited into the material as a charged particle passes through it. The differential energy lost by a particle as it passes through matter is given by the Bethe-Bloche formula:

$$\frac{dE}{dx} = -2\pi N_a r_e^2 m_e c^2 \rho \frac{Z}{A} \frac{z^2}{\beta^2} [ln(\frac{2m_e\gamma^2c^2\beta^2W_{max}}{I^2}) - 2\beta^2 - \delta]$$

dE/dx was calculated for various materials using a C++ program (see appendix 2) and the results are summarized in Table 16. Further material properties are summarized in Tables 17 and 18.

Table 16: dE/dx for Candidate Foil Materials

	dE/dx [MeV/m]	dE/dx [J/m]
Ti	840.970	1.35E-010
Al	537.178	8.61E-011
V	1100.580	1.76E-010
Be	347.901	5.57E-011
C(I)	472.637	7.57E-011
Fe	1441.870	2.31E-010
Si	480.858	7.70E-011
Zr	1128.640	1.81E-010
Sn	1205.380	1.93E-010
Mo	1744.320	2.79E-010
Nb	1481.520	2.37E-010
Cr	1312.460	2.10E-010
Ti-6Al-4V	833.126	1.33E-010
Ti-$\beta 21s$	988.899	1.58E-010
Ti-15Mo-5Zr	990.856	1.59E-010

Table 17: Candidate Foil Materials Thermal Properties

	k [W/m/K]	α@$300K[K^{-1}]$	α@$523K[K^{-1}]$	α@$773K[K^{-1}]$	ϵ	c [J/kg/K]
Be	200	1.15E-005	1.45E-005	1.65E-005	0.61000	1825
C(I)	345	6.00E-007	6.00E-007	6.00E-007	0.90000	707.7
Ti-6Al-4V	6.7	8.60E-006	9.20E-006	1.00E-005	0.01	526.3
Ti-$\beta 21s$	7.5	7.06E-006	8.76E-006	9.38E-006	0.01	710
Ti-15Mo-5Zr	7.5	8.50E-006	9.20E-006	-	0.01	540

Table 18: Candidate Foil Materials Mechanical Properties

	E [GPa]	Yield Strength [MPa]	Tensile Strength [MPa]	Fatigue Strength [Mpa]	Transus T [K]	Poisson's Ratio
Be	303	240	370	160	1500	0.07-0.18
C(I)	20	-	80	-	3800	0.33
Ti-6Al-4V	110-140	800-1100	900-1170	140-700	1268	0.34
Ti-$\beta 21s$	105	1277-1373	1383-1473	500-800	1073	0.33
Ti-15Mo-5Zr	105	920-1330	960-1700	375-700	1000	0.33